International Journal of Material Science Innovations
Volume 03, Issue 03, Pages 97-113, 2015
ISSN 2289-4063

Investigation of the Effect of Liquid and air swirl velocity and liquid viscosity on the hollow cone spray atomization

Bahram Jalili[a*], Fathollah Ommi[a], Elyas Rostami[a]

[a] Tarbiat Modares University, Department of Mechanical Engineering, Tehran, Iran
* Corresponding author. Tel.:+989124031827;
E-mail address: bahramjalily@yahoo.com

A b s t r a c t

Keywords:

Growth rate,
Linear instability,
Atomization,
Swirl,
Viscosity.

Air-blast atomizers provide excellent atomization over a large range of fuel flow rates and very good penetration. In this study we consider an annular liquid sheet emanating from an air-blast atomizer subjected to inner and outer swirling air streams. A temporal stability analysis is carried out to model the atomization of a swirling viscous annular liquid sheet subject to axi-symmetric disturbances and inviscid swirling air streams. Numerical solutions to the dispersion equation under a wide range of flow conditions are carried out to investigate the effects of the liquid-gas swirling orientation on the maximum growth rate and its corresponding unstable wave number.

Accepted:20 July2012

1. Introduction

When a liquid is injected under pressure from a nozzle into a surrounding gas medium, a continuous liquid jet is formed. Because of its inherent instability or its inabi1ity to sustain itself against even small perturbations, to which an-physical system is subject, the liquid jet develops unstable waves, which amplify downstream, and eventually it disintegrates into a train of droplets. The process of the liquid jet breakup consists of two fundamental steps. The first step is that the jet breaks up into ligaments. The second is that the ligaments further disintegrate into fine droplets. This process of liquid jet breakup into ligaments and then ligaments into droplets of fine sizes is often referred to as liquid atomization. The nozzle from which the Iiquid emanates is called atomizer, and the cluster of fine droplets so produced is usually termed as a spray. Liquid atomization is of importance in numerous applications such as fuel injection

in engines, gas turbine engines, industrial furnaces, agricultural sprays [1]. The stability of liquid jets and sheets has received much attention since the classical studies of Rayleigh and Squire. For authoritative reviews of liquid sheet and jet instability and breakup, readers are referred to a recent monograph by Lin [2] and reviews by Sirignano and Mehring [3]. Two limiting cases of the configuration considered here are available in the literature, viz., the swirling annular liquid sheet without air swirl considered by Panchagnula et al. [4] and the purely axially moving liquid sheet subjected to inner and outer air swirl considered by Liao et al. [5]. Panchagnula et al. [4] showed that liquid swirl reduces the wave number and the growth rate of the most-unstable disturbance at low swirl Weber number. However, at higher swirl, increasing the liquid swirl Weber number increases the range of unstable axial and circumferential modes and increases their growth rates. Liao et al. [5] compared the effectiveness of the inner and the outer air swirl and showed that a combination of the inner and outer air swirl is more effective than a single air swirl in enhancing the instability of the liquid sheet and in improving atomization, whereas the inner air swirl is more effective than the outer air swirl. Mehring and Sirignano [6] showed that liquid swirl can enhance wave growth of the unstable mode resulting in shorter breakup lengths using a non-linear analysis of a swirling, annular, axisymmetric liquid sheet in a void. The shortest breakup lengths were obtained with both the inner and the outer air stream co-rotating with the liquid. Chen et al. (2003) conducted a linear stability analysis for an annular viscous liquid jet subject to three dimensional disturbances moving in an inviscid, motionless gas phase [7]. Ibrahim et al. (2005) have conducted a temporal linear instability analysis of an inviscid, annular liquid sheet in an axially moving, inviscid gas medium [8]. Twin-fluid atomization is of significant fundamental and practical importance because of its extensive applications in pharmaceutical and chemical processing. Spray drying operations, power generation and propulsion systems. The formation and characteristics of sprays are strongly affected by the breakup process of the annular liquid jets. Therefore, the development and growth of unstable waves on the annular liquid jet Subject to inner and/or outer gas streams are investigated in this thesis theoretically by using the linear instability analysis.

2. Formulation for Linear Stability Analysis

2.1. Model Assumptions

The stability model considers a swirling viscous annular liquid sheet subject swirling airstreams as shown in Fig. 1. Gas phases are assumed to be inviscid and incompressible. The basic flow velocities for liquid, inner gas and outer gas are assumed to be $(U_l, 0, A_l r)$, $(U_i, 0, \Omega r)$, $(U_o, 0, A_o r)$ respectively. Inner gas swirl profile is assumed to be solid body rotation and outer gas swirl profile is of free vortex type.

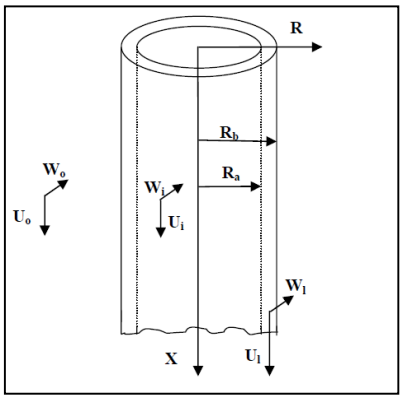

Fig. 1: Annular swirling viscous liquid sheet subject to swirling airstreams

Sheet instability occurs due to the growth of unstable waves at the liquid gas interface. The growth rates of these unstable waves are governed by fluid properties, nozzle geometry and competition of forces acting on the interface including viscous, pressure, inertial, surface tension, and centrifugal force. There exists a dominant or most unstable wave number corresponding to the maximum growth rate. The maximum growth rate and the most unstable wave number can be related to the breakup length and the mean droplet diameter, respectively. A temporal linear instability analysis is conducted to determine the maximum growth rate and the most unstable wave number.

2.2. Linearized Disturbance Equations

The governing equations for viscous fluid flows in cylindrical coordinate system are :

Continuity:

$$\frac{V}{r}+\frac{\partial V}{\partial r}+\frac{1}{r}\frac{\partial W}{\partial \theta}+\frac{\partial U}{\partial x}=0 \qquad (1)$$

Momentum:

$$\frac{\partial U}{\partial t}+U\frac{\partial U}{\partial x}+V\frac{\partial U}{\partial r}+\frac{1}{r}W\frac{\partial U}{\partial \theta}=-\frac{1}{\rho}\frac{\partial P}{\partial x}+\nu\left(\frac{\partial^2 U}{\partial r^2}+\frac{1}{r}\frac{\partial U}{\partial r}+\frac{1}{r^2}\frac{\partial^2 U}{\partial \theta^2}+\frac{\partial^2 U}{\partial x^2}\right) \qquad (2)$$

$$\frac{\partial V}{\partial t}+U\frac{\partial V}{\partial x}+V\frac{\partial V}{\partial r}+\frac{1}{r}W\frac{\partial V}{\partial \theta}-\frac{W^2}{r}=-\frac{1}{\rho}\frac{\partial P}{\partial r}+\nu\left(\frac{\partial^2 V}{\partial r^2}+\frac{1}{r}\frac{\partial V}{\partial r}+\frac{1}{r^2}\frac{\partial^2 V}{\partial \theta^2}-\frac{V}{r^2}-\frac{2}{r^2}\frac{\partial W}{\partial \theta}+\frac{\partial^2 V}{\partial x^2}\right) \qquad (3)$$

$$\frac{\partial W}{\partial t}+U\frac{\partial W}{\partial x}+V\frac{\partial W}{\partial r}+\frac{1}{r}W\frac{\partial W}{\partial \theta}+\frac{VW}{r}=-\frac{1}{\rho r}\frac{\partial P}{\partial \theta}+\nu\left(\frac{\partial^2 W}{\partial r^2}+\frac{1}{r}\frac{\partial W}{\partial r}+\frac{1}{r^2}\frac{\partial^2 W}{\partial \theta^2}-\frac{W}{r^2}+\frac{2}{r^2}\frac{\partial V}{\partial \theta}+\frac{\partial^2 W}{\partial x^2}\right) \qquad (4)$$

In order to obtain the linearized disturbance equations, let

$$U=\bar{U}+u\ ,\ V=v\ ,\ W=\bar{W}+w\ ,\ p=\bar{P}+p' \qquad (5)$$

Where, the over bar represents the mean flow quantities and *u*, *v*, *w* and p' indicates disturbance. The disturbances are assumed to be of the form,

$$(u,v,w,p')=\begin{pmatrix}\hat{u}(r),\hat{v}(r),\\ \hat{w}(r),\hat{p}(r)\end{pmatrix}e^{i(kx+n\theta-\omega t)} \qquad (6)$$

Where ^ indicates the disturbance amplitude which is a function of r only. For linear temporal instability analysis, wave numbers *k* and *n* are real, while the frequency ω is complex. The maximum value of imaginary ω represents the maximum growth rate and the corresponding

value of k represents the most unstable wave number. The displacement disturbance at the inner and outer interfaces are given by the following equations,

$$\eta_i(x,\theta,t) = \hat{\eta}_i e^{i(kx+n\theta-\omega t)+i\phi} \tag{7}$$

$$\eta_o(x,\theta,t) = \hat{\eta}_o e^{i(kx+n\theta-\omega t)} \tag{8}$$

Here ϕ indicates the phase difference between the displacement at the inner and the outer interface. For plane liquid sheets, ϕ either zero or π. A zero phase difference represents the sinuous mode while a phase difference of π represents the varicose mode. Substituting Eq. (5) into Eq. (1), (2), (3) and (4), subtracting the mean flow equations and neglecting the second order terms, we get the linearized equation for velocity and pressure disturbances as:

Continuity:

$$\frac{\partial u}{\partial x} + \frac{v}{r} + \frac{\partial v}{\partial r} + \frac{1}{r}\frac{\partial w}{\partial \theta} = 0 \tag{9}$$

Momentum:

$$\frac{\partial u}{\partial t} + U_l \frac{\partial u}{\partial x} + \frac{A_l}{r^2}\frac{\partial u}{\partial \theta} = -\frac{1}{\rho_l}\frac{\partial p'}{\partial x} + \nu\left(\frac{\partial^2 u}{\partial r^2} + \frac{1}{r}\frac{\partial u}{\partial r} + \frac{1}{r^2}\frac{\partial^2 u}{\partial \theta^2} + \frac{\partial^2 u}{\partial x^2}\right) \tag{10}$$

$$\frac{\partial v}{\partial t} + U_l \frac{\partial v}{\partial x} + \frac{A_l}{r^2}\frac{\partial v}{\partial \theta} - \frac{2A_l w}{r^2} = -\frac{1}{\rho_l}\frac{\partial p'}{\partial r} + \nu\left(\frac{\partial^2 v}{\partial r^2} + \frac{1}{r}\frac{\partial v}{\partial r} + \frac{1}{r^2}\frac{\partial^2 v}{\partial \theta^2} - \frac{v}{r^2} - \frac{2}{r^2}\frac{\partial w}{\partial \theta} + \frac{\partial^2 v}{\partial x^2}\right) \tag{11}$$

$$\frac{\partial w}{\partial t} + U_l \frac{\partial w}{\partial x} + \frac{A_l}{r^2}\frac{\partial w}{\partial \theta} = -\frac{1}{\rho_l r}\frac{\partial p'}{\partial \theta} + \nu\left(\frac{\partial^2 w}{\partial r^2} + \frac{1}{r}\frac{\partial w}{\partial r} + \frac{1}{r^2}\frac{\partial^2 w}{\partial \theta^2} - \frac{w}{r^2} + \frac{2}{r^2}\frac{\partial v}{\partial \theta} + \frac{\partial^2 w}{\partial x^2}\right) \tag{12}$$

Similarly the linearized disturbance equations for gas flow in component form are given as:

Continuity:

$$\frac{\partial u}{\partial x} + \frac{v}{r} + \frac{\partial v}{\partial r} + \frac{1}{r}\frac{\partial w}{\partial \theta} = 0 \tag{13}$$

Momentum:

$$\frac{\partial u}{\partial t} + U_j \frac{\partial u}{\partial x} + \frac{W_j}{r}\frac{\partial u}{\partial \theta} = -\frac{1}{\rho_j}\frac{\partial p'_j}{\partial x} \tag{14}$$

$$\frac{\partial v}{\partial t} + U_j \frac{\partial v}{\partial x} + \frac{W_j}{r}\frac{\partial v}{\partial \theta} - \frac{2W_j w}{r} = -\frac{1}{\rho_j}\frac{\partial p'_j}{\partial r} \tag{15}$$

$$\frac{\partial w}{\partial t} + U_j \frac{\partial w}{\partial x} + v\frac{\partial W_j}{\partial r} + \frac{W_j}{r}\frac{\partial w}{\partial \theta} + \frac{W_j v}{r} = -\frac{1}{\rho_j r}\frac{\partial p'_j}{\partial \theta} \tag{16}$$

Where $j = i,o$ and $Wi = \Omega r$, $Wo = Ao\, r$

Inorder to determine the effect of the various forces, properties of fluids and other geometric parameters, the following non-dimensional parameters are introduced:

$$We_l=\frac{\rho_l U_l^{\,2}R_b}{\sigma}\ ,\ We_i=\frac{\rho_i U_i^{\,2}R_b}{\sigma}\ ,We_o=\frac{\rho_o U_o^{\,2}R_b}{\sigma}\ ,$$

$$We_s=\frac{\rho_l W_l^{\,2}R_b}{\sigma},We_{si}=\frac{\rho_i W_i^{\,2}R_b}{\sigma}\ ,We_{so}=\frac{\rho_o W_o^{\,2}R_b}{\sigma},$$

$$\mathrm{Re}=\frac{\rho_l U_l R_b}{\mu}\ \ ,g_i=\frac{\rho_i}{\rho_l}\ \ ,\ \ g_o=\frac{\rho_o}{\rho_l}\ ,\bar{k}=kR_b,$$

$$\bar{\omega}=\frac{\omega R_b}{U_l}\ ,\ \frac{U_i}{U_l}=\sqrt{\frac{We_i}{We_l}\frac{1}{g_i}}\ ,\ \frac{U_o}{U_l}=\sqrt{\frac{We_o}{We_l}\frac{1}{g_o}}\ \ ,$$

$$\frac{A_l}{U_l R_b}=\sqrt{\frac{We_s}{We_l}}\ ,\frac{A_o}{U_l R_b}=\sqrt{\frac{We_{so}}{We_l}\frac{1}{g_o}}\ ,h=\frac{R_a}{R_b}$$

$$\frac{\Omega R_b}{U_l}=\sqrt{\frac{We_{si}}{We_l}\frac{1}{g_i}}\ \ ,\bar{s}=\left(\bar{k}^2+\mathrm{Re}\left(-i\bar{\omega}+i\bar{k}\right)\right)^{\frac{1}{2}}$$

Weber numbers for the fluid, the gas inside and outside were defined in modes the axial velocity and rotational. $h,\ g_{i,\,o}\ ,\ \bar{k},\ \bar{\omega},\ \mathrm{Re}$ Respectively are the radius ratio, the density ratio of gas to liquid, dimensionless wave number, dimensionless growth rate, Reynolds number of flow.

2.3. Boundary Conditions

The following boundary conditions are necessary to solve the linearized disturbance equations.

Kinematic Boundary conditions:

Liquid:

$$v=\frac{\partial\eta_i}{\partial t}+\frac{1}{r^2}\frac{\partial\eta_i}{\partial\theta}\sqrt{\frac{We_s}{We_l}}+\frac{\partial\eta_i}{\partial x}\quad at\ \ r=h \tag{17}$$

$$v=\frac{\partial\eta_o}{\partial t}+\frac{1}{r^2}\frac{\partial\eta_o}{\partial\theta}\sqrt{\frac{We_s}{We_l}}+\frac{\partial\eta_o}{\partial x}\quad at\quad r=1 \tag{18}$$

Inner Gas:

$$v_i=\frac{\partial\eta_i}{\partial t}+\frac{\partial\eta_i}{\partial\theta}\sqrt{\frac{We_{si}}{We_l}\frac{1}{g_i}}+\frac{\partial\eta_i}{\partial x}\sqrt{\frac{We_i}{We_l}\frac{1}{g_i}}\ at\ r=h \tag{19}$$

Outer Gas:

$$v_o=\frac{\partial\eta_o}{\partial t}+\frac{1}{r^2}\frac{\partial\eta_o}{\partial\theta}\sqrt{\frac{We_{so}}{We_l}\frac{1}{g_o}}+\frac{\partial\eta_o}{\partial x}\sqrt{\frac{We_o}{We_l}\frac{1}{g_o}}\quad at\quad r=1 \tag{20}$$

Due to the inviscid assumption for the gas streams in the axial and azimuthal directions, viscous stress at the liquid-gas interface is zero. This is expressed as:

$$\frac{\partial u}{\partial r}+\frac{\partial v}{\partial x}=0\qquad at\ \ r=h\ ,1 \tag{21}$$

$$\frac{\partial w}{\partial r}-\frac{w}{r}+\frac{1}{r}\frac{\partial v}{\partial\theta}=0\quad at\ \ r=h\ ,1 \tag{22}$$

The dynamic boundary conditions require that the forces in the normal direction be balanced. These include pressure, surface tension, inertial, centrifugal and viscous force. Mathematically they are expressed as:

$$p_l'-p_i'=\frac{1}{h^2We_l}\left(\eta_i+\frac{\partial^2\eta_i}{\partial\theta^2}+h^2\frac{\partial^2\eta_i}{\partial x^2}\right)+h\frac{We_{si}}{We_l}\eta_i-\frac{We_s}{We_l}\frac{\eta_i}{h^3}+\frac{2}{\mathrm{Re}}\frac{\partial v}{\partial r}\qquad at\ r=h \tag{23}$$

$$p_l'-p_o'=\frac{-1}{We_l}\left(\eta_o+\frac{\partial^2\eta_o}{\partial\theta^2}+\frac{\partial^2\eta_o}{\partial x^2}\right)+\frac{We_{so}}{We_l}\eta_o-\frac{We_s}{We_l}\eta_o+\frac{2}{\mathrm{Re}}\frac{\partial v}{\partial r}\qquad at\ r=1 \tag{24}$$

2.4. Pressure disturbance inside the liquid sheet

Here the subscripts 1 and 2 represent the inviscid and the viscous parts of the velocity perturbations. Now equations for the two parts can be written as:

Inviscid:

$$\hat{u}_1\left(i\bar{k}\right)+\frac{d\hat{v}_1}{dr}+\frac{\hat{v}_1}{r}=0 \tag{25}$$

$$\hat{u}_1\left(-i\bar{\omega}+i\bar{k}\right)=-i\bar{k}\hat{p} \tag{26}$$

$$\hat{v}_1\left(-i\bar{\omega}+i\bar{k}\right)=-\frac{d\hat{p}}{dr} \tag{27}$$

Viscous:

$$\hat{u}_2\left(i\bar{k}\right)+\frac{d\hat{v}_2}{dr}+\frac{\hat{v}_2}{r}=0 \tag{28}$$

$$\hat{u}_2\left(-i\,\bar{\omega}+i\bar{k}\right)=\frac{1}{\mathrm{Re}}\left(\frac{d^2\hat{u}_2}{dr^2}+\frac{1}{r}\frac{d\hat{u}_2}{dr}-\frac{\hat{u}_2}{r^2}\left(\bar{k}^2r^2\right)\right) \quad (29)$$

$$\hat{v}_2\left(-i\,\bar{\omega}+i\bar{k}\right)=\frac{1}{\mathrm{Re}}\left(\frac{d^2\hat{v}_2}{dr^2}+\frac{1}{r}\frac{d\hat{v}_2}{dr}-\frac{\hat{v}_2}{r^2}\left(\bar{k}^2r^2+1\right)\right) \quad (30)$$

Terms of the fluid velocity can be written as follows:

$$\hat{u}=\hat{u}_1+\hat{u}_2\,,\hat{v}=\hat{v}_1+\hat{v}_2 \quad (31)$$

Differentiating (26) with respect to r and eliminating $p\hat{}$ from (26) and (27), we get:

$$\hat{v}_1=\frac{1}{i\bar{k}}\frac{d\hat{u}_1}{dr} \quad (32)$$

Substituting (32) in (25), we have:

$$\left(\frac{d^2\hat{u}_1}{dr^2}+\frac{1}{r}\frac{d\hat{u}_1}{dr}-\frac{\hat{u}_1}{r^2}\left(\bar{k}^2r^2\right)\right)=0 \quad (33)$$

The above equation is a Bessel equation which has a solution of the form:

$$\hat{u}_1=C_1I_0\left(\bar{k}r\right)+C_2K_0\left(\bar{k}r\right) \quad (34)$$

Substituting (34) in (32) and (26), we obtain:

$$\hat{v}_1=-i\;C_1I_1\left(\bar{k}r\right)+i\;C_2K_1\left(\bar{k}r\right) \quad (35)$$

$$\hat{p}=\frac{\bar{\omega}-\bar{k}}{\bar{k}}\left(C_1I_0\left(\bar{k}r\right)+C_2K_0\left(\bar{k}r\right)\right) \quad (36)$$

By applying this method over Equations of (28) to (30), The velocity terms are obtained as follows:

$$\hat{u}=C_1I_0\left(\bar{k}r\right)+C_2K_0\left(\bar{k}r\right)+C_3I_0\left(\bar{s}r\right)+C_4K_0\left(\bar{s}r\right) \quad (37)$$

$$\hat{v}=-i\;C_1I_1\left(\bar{k}r\right)+i\;C_2K_1\left(\bar{k}r\right)+C_5I_1\left(\bar{s}r\right)+C_6K_1\left(\bar{s}r\right) \quad (38)$$

Using the boundary conditions (Eq. (17), (18) and (21)) the constants *C*1, C2 to *C*6 are determined and by substituting them inside Equation (36), the pressure disturbance inside the liquid sheet can be expressed as,

$$p_l'=\frac{\bar{\omega}-\bar{k}}{\bar{k}}\begin{pmatrix}C_1I_0\left(\bar{k}r\right)+\\C_2K_0\left(\bar{k}r\right)\end{pmatrix}e^{i\left(\bar{k}x+n\theta-\bar{\omega}t\right)} \quad (39)$$

The coefficients are given by the following equations,

$$\begin{aligned}C_1=&\frac{-(\bar{k}^3\hat{\eta}_ie^{i\varphi}K_1(\bar{k}h)-\bar{k}^2\bar{\omega}\hat{\eta}_ie^{i\varphi}K_1(\bar{k}h))}{(-K_1(\bar{k}h)I_1(\bar{k})+I_1(\bar{k}h)K_1(\bar{k}))(\bar{k}^2-\bar{s}^2)}\\&-\frac{(\bar{k}\,\bar{s}^2\hat{\eta}_ie^{i\varphi}K_1(\bar{k}h)-\bar{s}^2\bar{\omega}\hat{\eta}_ie^{i\varphi}K_1(\bar{k}h))}{(-K_1(\bar{k}h)I_1(\bar{k})+I_1(\bar{k}h)K_1(\bar{k}))(\bar{k}^2-\bar{s}^2)}\\&-\frac{(\bar{s}^2\bar{\omega}\hat{\eta}_o\,K_1(\bar{k})-\bar{k}^3\hat{\eta}_oK_1(\bar{k}))}{(-K_1(\bar{k}h)I_1(\bar{k})+I_1(\bar{k}h)K_1(\bar{k}))(\bar{k}^2-\bar{s}^2)}\\&-\frac{(\bar{k}^2\,\bar{\omega}\hat{\eta}_oK_1(\bar{k})-\bar{s}^2\hat{\eta}_o\bar{k}K_1(\bar{k}))}{(-K_1(\bar{k}h)I_1(\bar{k})+I_1(\bar{k}h)K_1(\bar{k}))(\bar{k}^2-\bar{s}^2)}\end{aligned} \quad (40)$$

$$\begin{aligned}C_2=&\frac{-(-\bar{k}^3\hat{\eta}_oI_1(\bar{k})+\bar{k}^3\hat{\eta}_ie^{i\varphi}I_1(\bar{k}h))}{(-K_1(\bar{k}h)I_1(\bar{k})+I_1(\bar{k}h)K_1(\bar{k}))(\bar{k}^2-\bar{s}^2)}\\&-\frac{(\bar{k}^2\bar{\omega}\hat{\eta}_oI_1(\bar{k})-\bar{k}^2\bar{\omega}\hat{\eta}_ie^{i\varphi}I_1(\bar{k}h))}{(-K_1(\bar{k}h)I_1(\bar{k})+I_1(\bar{k}h)K_1(\bar{k}))(\bar{k}^2-\bar{s}^2)}\\&-\left(\frac{-\bar{s}^2\bar{k}\,\hat{\eta}_o\,I_1(\bar{k})+\bar{k}\,\hat{\eta}_i\bar{s}^2e^{i\varphi}I_1(\bar{k}h)}{(-K_1(\bar{k}h)I_1(\bar{k})+I_1(\bar{k}h)K_1(\bar{k}))(\bar{k}^2-\bar{s}^2)}\right)\\&-\frac{(\bar{s}^2\bar{\omega}\hat{\eta}_oI_1(\bar{k})-\bar{s}^2\bar{\omega}\hat{\eta}_ie^{i\varphi}I_1(\bar{k}h))}{(-K_1(\bar{k}h)I_1(\bar{k})+I_1(\bar{k}h)K_1(\bar{k}))(\bar{k}^2-\bar{s}^2)}\end{aligned} \quad (41)$$

$$\begin{aligned}C_3=&\frac{2\bar{s}^2\bar{k}\,(-\bar{k}\,\hat{\eta}_oK_1(\bar{s})+\bar{k}\,\hat{\eta}_ie^{i\varphi}K_1(\bar{s}h))}{(\bar{k}^2-\bar{s}^2)(-I_1(\bar{s})K_1(\bar{s}h)+K_1(\bar{s})I_1(\bar{s}h))}\\&+\frac{2\bar{s}^2\bar{k}\,(-\hat{\eta}_ie^{i\varphi}\bar{\omega}K_1(\bar{s}h)+\hat{\eta}_o\bar{\omega}K_1(\bar{s}))}{(\bar{k}^2-\bar{s}^2)(-I_1(\bar{s})K_1(\bar{s}h)+K_1(\bar{s})I_1(\bar{s}h))}\end{aligned} \quad (42)$$

$$C_4=\frac{-2\bar{s}^2\bar{k}\,(\bar{k}\,\hat{\eta}_ie^{i\varphi}I_1(\bar{s}h)-\bar{\omega}\hat{\eta}_ie^{i\varphi}I_1(\bar{s}h)-\hat{\eta}_o\bar{k}I_1(\bar{s})+\hat{\eta}_o\bar{\omega}I_1(\bar{s}))}{-\bar{k}^2I_1(\bar{s})K_1(\bar{s}h)+\bar{s}^2I_1(\bar{s})K_1(\bar{s}h)+\bar{k}^2K_1(\bar{s})I_1(\bar{s}h)-\bar{s}^2K_1(\bar{s})I_1(\bar{s}h)} \quad (43)$$

$$\begin{aligned}C_5=&\frac{-2i\;\bar{k}^2(-\bar{k}\,\hat{\eta}_oK_1(\bar{s})+\bar{k}\,\hat{\eta}_ie^{i\varphi}K_1(\bar{s}h))}{(\bar{k}^2-\bar{s}^2)(-I_1(\bar{s})K_1(\bar{s}h)+K_1(\bar{s})I_1(\bar{s}h))}\\&-\frac{2i\;\bar{k}^2(-\hat{\eta}_ie^{i\varphi}\bar{\omega}K_1(\bar{s}h)+\hat{\eta}_o\bar{\omega}K_1(\bar{s}))}{(\bar{k}^2-\bar{s}^2)(-I_1(\bar{s})K_1(\bar{s}h)+K_1(\bar{s})I_1(\bar{s}h))}\end{aligned} \quad (44)$$

$$C_6=\frac{2i\;\bar{k}^2(\bar{k}\,\hat{\eta}_ie^{i\varphi}I_1(\bar{s}h)-\bar{\omega}\hat{\eta}_ie^{i\varphi}I_1(\bar{s}h)-\hat{\eta}_o\bar{k}I_1(\bar{s})+\hat{\eta}_o\bar{\omega}I_1(\bar{s}))}{-\bar{k}^2I_1(\bar{s})K_1(\bar{s}h)+\bar{s}^2I_1(\bar{s})K_1(\bar{s}h)+\bar{k}^2K_1(\bar{s})I_1(\bar{s}h)-\bar{s}^2K_1(\bar{s})I_1(\bar{s}h)} \quad (45)$$

2.5. Pressure disturbance in inner and outer gas phase

Linear Continuity and momentum equations and dimensionless for gas phase can be written as follows:

$$\hat{u}\left(i\bar{k}\right)+\frac{d\hat{v}}{dr}+\frac{\hat{v}}{r}=0 \tag{46}$$

$$\hat{u}\left(-i\bar{\omega}+i\bar{k}\sqrt{\frac{We_j}{We_l}\frac{1}{g_j}}\right)=-\frac{1}{g_j}i\bar{k}\hat{p} \tag{47}$$

$$\hat{v}\left(-i\bar{\omega}+i\bar{k}\sqrt{\frac{We_j}{We_l}\frac{1}{g_j}}\right)=-\frac{1}{g_j}\frac{d\hat{p}}{dr} \tag{48}$$

The pressure disturbance inside the inner and outer gas are calculated such the pressure disturbance inside the liquid sheet that by refraining the related operations.

Pressure disturbance in inner gas:

$$p_i'=\frac{g_i\left(\bar{\omega}-\bar{k}\sqrt{\frac{We_i}{We_l}\frac{1}{g_i}}\right)^2\hat{\eta}_i e^{i\varphi}}{\bar{k}I_1\left(\bar{k}h\right)}I_0\left(\bar{k}h\right)e^{i\left(\bar{k}x-\bar{\omega}t\right)} \tag{49}$$

Pressure disturbance in outer gas:

$$p_o'=-\frac{g_o\left(\bar{\omega}-\bar{k}\sqrt{\frac{We_o}{We_l}\frac{1}{g_o}}\right)^2\hat{\eta}_o}{\bar{k}K_1\left(\bar{k}\right)}K_0\left(\bar{k}\right)e^{i\left(\bar{k}x-\bar{\omega}t\right)} \tag{50}$$

Where, $I_n(v)$, $K_n(v)$ are the n^{th} order modified Bessel Function of first and second kind respectively. The Nonlinear dimensionless dispersion equation is obtained by substituting the pressure disturbances inside Equations (23) and (24) and with Remove the common factors. The Final Dispersion Equation was solved numerically using the secant method.

$$f\begin{pmatrix}\bar{\omega},\bar{k},\bar{s},g_i,g_o,\mathrm{Re},We_l,We_i,\\We_o,We_s,We_{si},We_{so},h\end{pmatrix}=0 \tag{51}$$

Unlike the inviscid case, the final dispersion equation does not have a closed form solution and is solved numerically using *Mathematica*™. The Secant method is used where two starting complex guess values are required to determine the roots of the dimensionless dispersion equation. Results from the inviscid case are taken as starting guess values. By varying the value of $\bar{k}$, we solve for the root with the maximum imaginary part that represents the maximum growth rate of disturbance corresponding to the most unstable wave number and the primary breakup of spray is discussed.

2.6. Breakup Mechanism

If surface disturbance at breakup time reach to η_b , breakup time (τ), Is calculated from the following equation [9]:

$$\eta_b=\eta_0\exp(\omega\tau)\Rightarrow\tau=\frac{1}{\omega}\ln(\frac{\eta_b}{\eta_0}) \tag{52}$$

In the above equation, ω is the maximum wave growth rate that is calculated by solving the final distribution equation and $\ln(\frac{\eta_b}{\eta_0})=12$ is placed the experimental results Dombrowski and Hopper [10]. Also primary breakup lengths of layer will be as follows:

$$L_b=V_1\tau=\frac{V_1}{\omega}\ln(\frac{\eta_b}{\eta_0})=\frac{12V_1}{\omega} \tag{53}$$

In the above equation, V_1 is the absolute velocity of the fluid and L_b is the primary breakup length of fluid layer. Because in equation (51)

dimensionless wave growth rate to be achieved, so with the following procedure will become:

$$\bar{\omega} = \frac{\omega R_b}{V_1} \Rightarrow \omega = \frac{\bar{\omega} V_1}{R_b} \Rightarrow L_b = \frac{12 R_b}{\bar{\omega}} \quad (54)$$

In the above equation, R_b is Outer radius of the liquid annular layer and $\bar{\omega}$ is the dimensionless wave growth rate. Also ligaments diameter that formed at the point of break Caused of the jet break or layers is obtained from the following equation [9]:

$$d_L = \sqrt{\frac{16 h_s}{k}} \quad (55)$$

In the previous equation, d_L is ligament diameter and k is Wave number corresponding to the maximum wave growth rate and h_s is half of the layer thickness that is obtained from the following equations:

$$\bar{k} = k R_b \Rightarrow k = \frac{\bar{k}}{R_b}; h_s = \frac{(R_b - R_a)}{2} \quad (56)$$

Consequently, ligament diameter is calculated as follows:

$$d_L = \sqrt{\frac{16 h_s R_b}{\bar{k}}} \quad (57)$$

Droplet diameter Caused of the viscous fluid ligament break can be obtained as follows [9]:

$$d_D = 1.88 d_L (1 + 3Oh)^{\frac{1}{6}} \quad (58)$$

In the above equation, Oh is Viscosity to liquid surface tension ratios and is obtained from the following equation:

$$Oh = \frac{\mu_l}{(\rho_l \sigma d_L)^{\frac{1}{2}}} \quad (59)$$

Solve the equation (51) is Introduction to achieve the primary breakup lengths relationship (equation (54)). To reach the Ligament and droplet diameter should be used Wave number corresponding to the maximum wave growth rate from equation (51). From equation (54) it can be concluded that with increases the maximum wave growth rate is reduced the primary breakup lengths. From equation (57) with increases the Wave number corresponding to the wave growth rate is reduced the ligament diameter and also is reduced the droplet diameter (From equation (58)).

3. Result and Discussion

3.1. Effect of Liquid swirl velocity

Figure 2 shows the damping effect of liquid viscosity. At a constant Weber number, change in Re corresponds to a change in liquid viscosity. Higher values of Reynolds number correspond to lower viscosity. Hence the maximum growth rate increases with Reynolds number eventually reaching the growth rate for an inviscid case for Re=1000. This would imply that higher liquid growth rate would lead to shorter breakup lengths and smaller droplets. The maximum growth rate increases, Primary break up length, ligament diameter and droplet diameter decreases and improves combustion and reduces emissions and fuel consumption. So Fig. 3 has a shorter Primary break up length compared to Fig. 2. Also ligament diameter and droplet diameter of Fig. 3 is shorter than Fig. 2. In general, with increasing the wave

growth rate, Primary break up lengths and ligament diameter is reduced and thus the droplet diameter decreases. Also liquid viscosity has a negative effect on the Primary break up lengths and it Causes to become the increasing the Primary break up length on the other hand Viscosity increase causes to become increasing the Primary break up length. Also Viscosity increase causes to become increasing the ligament diameter and droplet diameter. The variations of growth rate with wave number for a liquid sheet with both axial and swirl velocity components are shown in Figs.3. The axial Weber number and the swirl Weber number are taken as equal. From Fig.3 it can be observed that the maximum growth rate and the most unstable wave number are significantly higher compared to their no swirl counterpart (Figs.2, respectively). This indicates that liquid swirl promotes instability at high Weber numbers. The figures also show that the damping effect of viscosity is stronger for a swirling sheet compared to that for a non-swirling sheet. At very high viscosity (Re = 10), the maximum growth rate for the swirling case are lower than that for a non-swirling case. The effect of liquid swirl (liquid swirl Weber numbers from 0 to 75) on the maximum growth rate and the most unstable axial wave number are shown in fig. 7. It is observed that liquid swirl has a dual effect on sheet instability. At low values of liquid swirl Weber numbers (0 to about 20), a stabilizing effect is seen. At low values of swirl, at the inner interface, the centrifugal forces due to liquid swirl tend to push the perturbed sheet back to its undisturbed state. As such, at low liquid swirl Weber number, liquid swirl tends to have a stabilizing effect on the liquid sheet. The centrifugal force due to liquid swirl at the outer interface tends to push a perturbed interface further outward and exhibits a destabilizing effect. The disturbance growth rate increases with increasing liquid swirl Weber number at high liquid swirl.

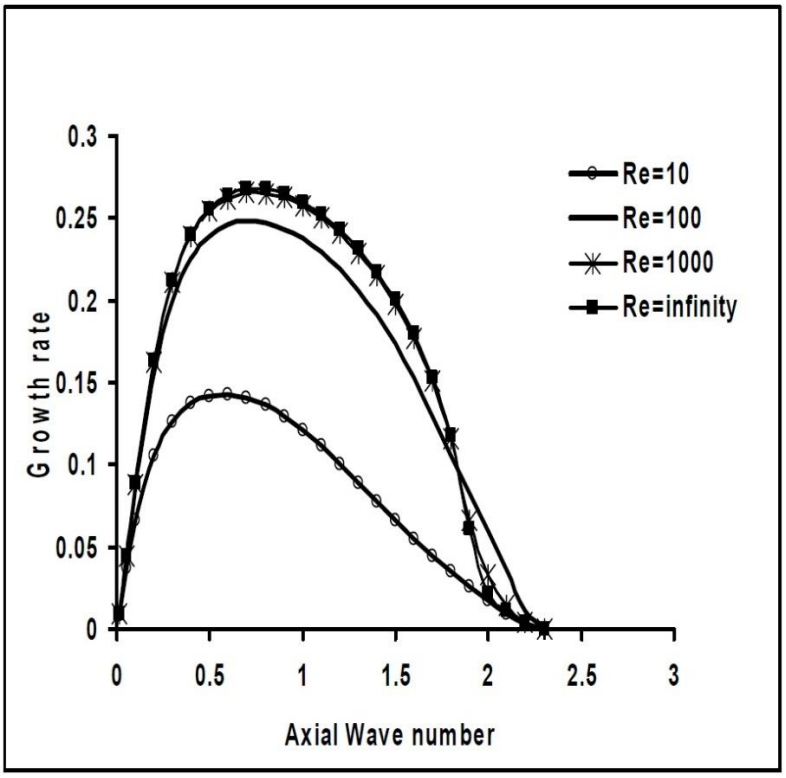

Fig. 2: Dispersion diagram at We_l=1000, g_i=g_o=0.00123, h=0.95

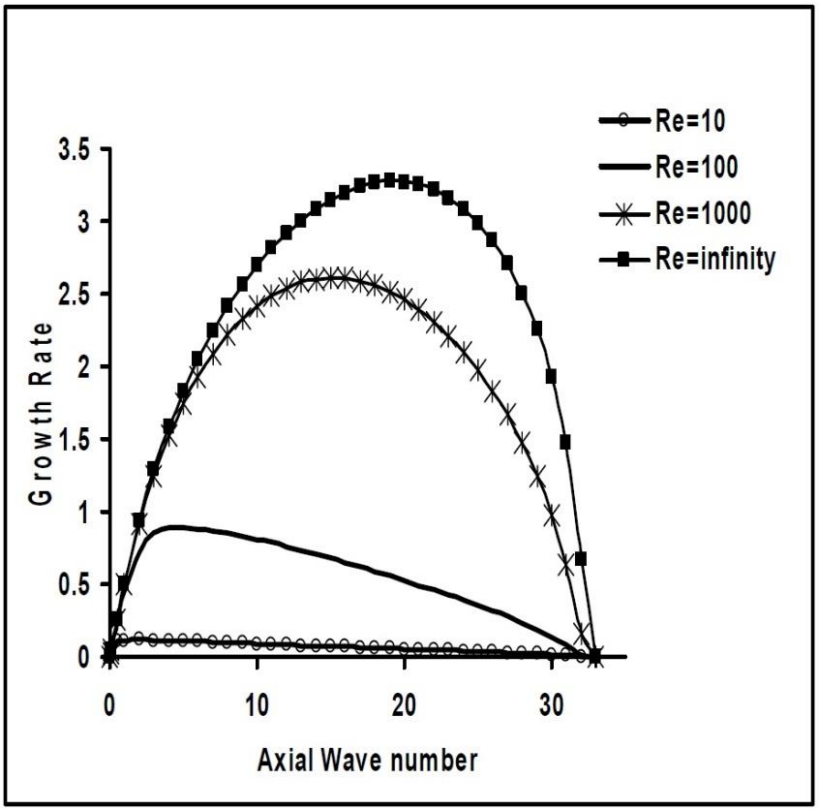

Fig. 3: Dispersion diagram at We_l= We_s =1000, g_i=g_o=0.00123, h=0.95

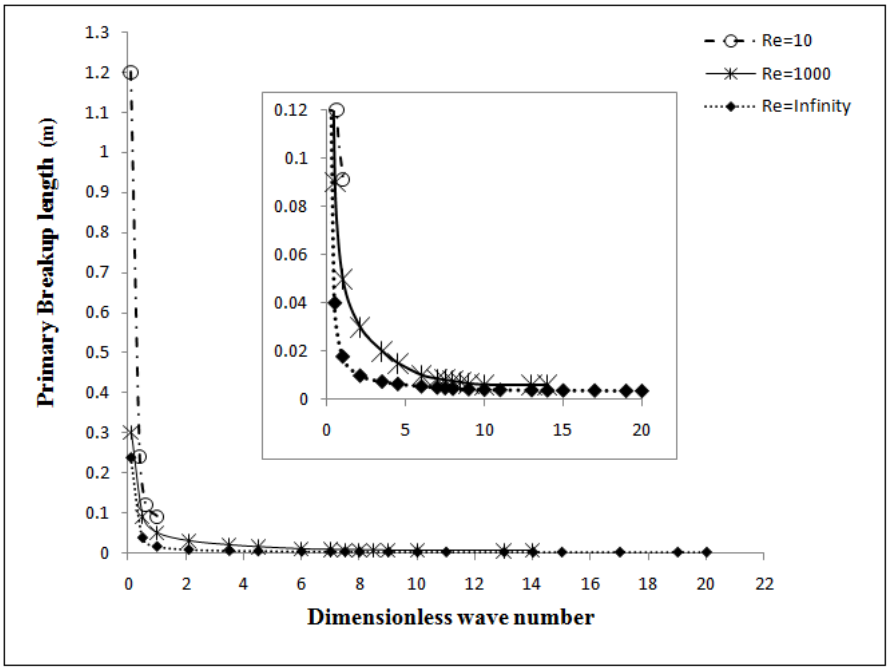

Fig. 3: The Effect of Liquid Viscosity on the primary break up of spray at $We_l=We_s=1000$, $g_i=g_o=0.00123$, h=0.95

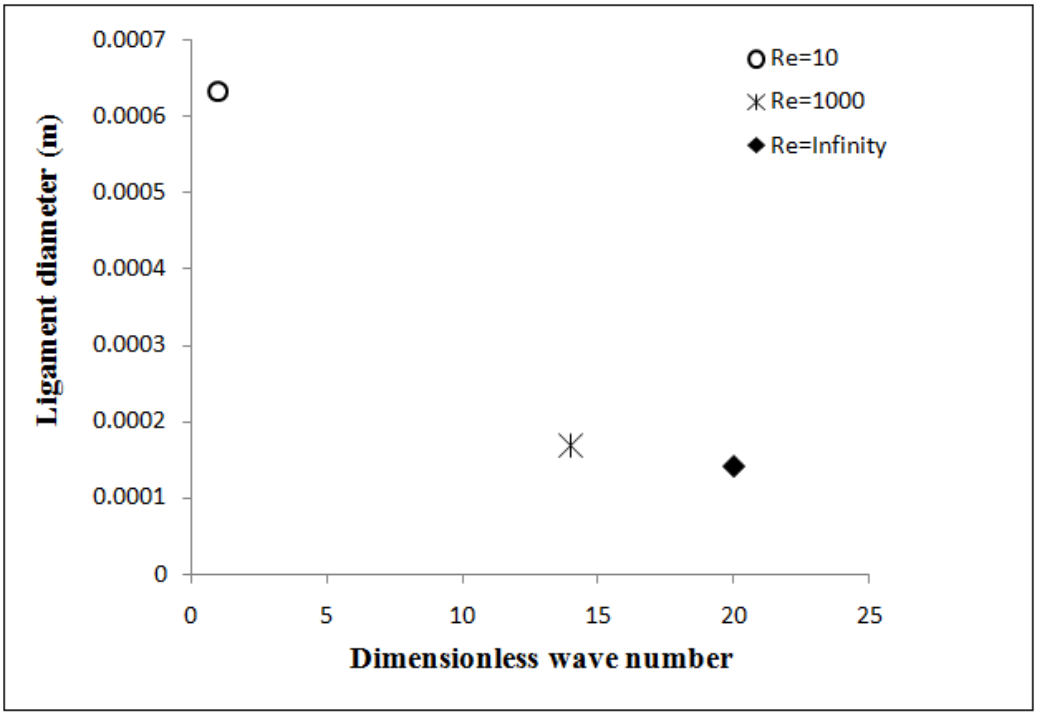

Fig. 4: The Effect of Liquid Viscosity on Ligament diameter at $We_l=We_s=1000$, $g_i=g_o=0.00123$, h=0.95

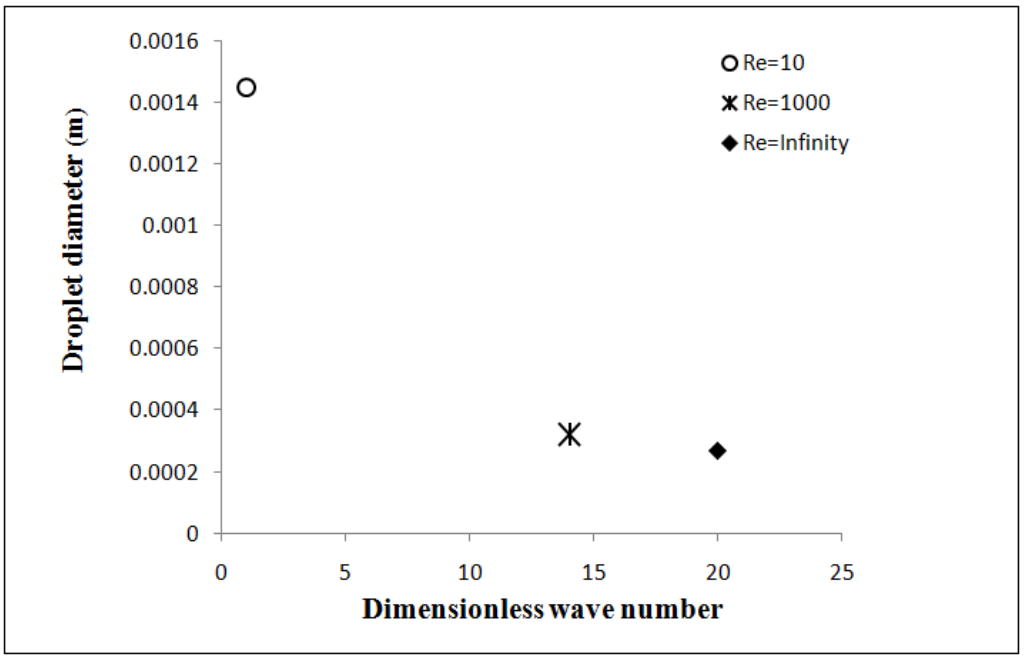

Fig. 5: The Effect of Liquid Viscosity on Droplet diameter at $We_l=We_s=1000$, $g_i=g_o=0.00123$, h=0.95

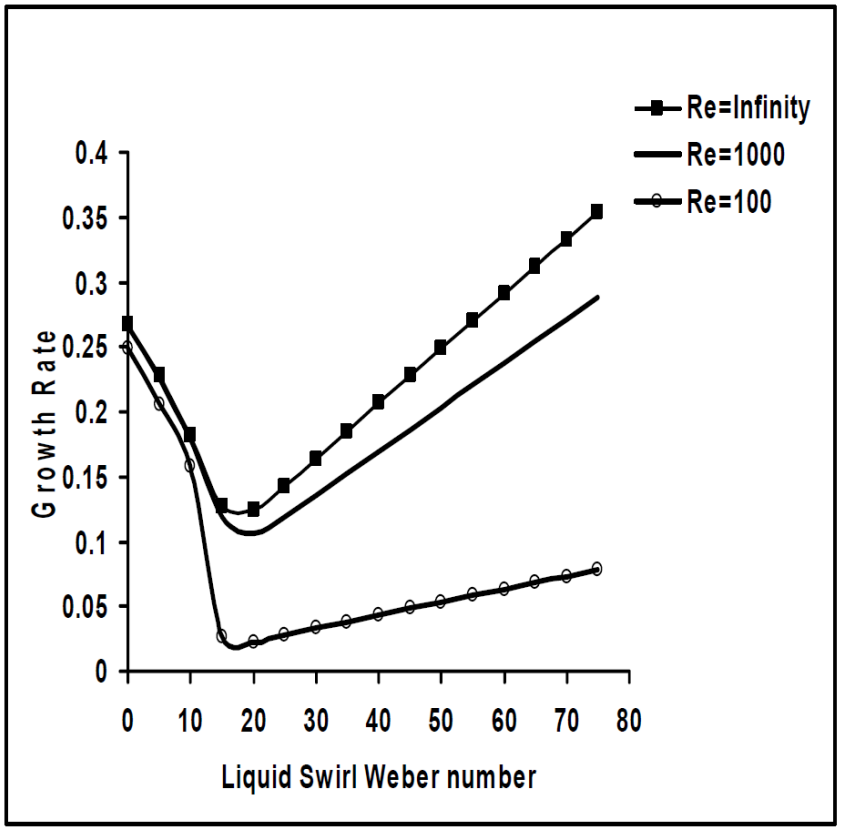

Fig. 7: Liquid Swirl Weber number Vs Growth Rate at $We_l=1000$, $g_i=g_o=0.00123$, h=0.95

3.2. Effect of air swirl

Figure 8 present the effect of axial gas velocities in the disintegration of swirling, annular liquid sheets. The combination of inner and outer air is more effective in destabilizing swirling liquid sheets than liquid sheet with both axial and swirl velocity (Fig. 3). The aerodynamic interaction at the liquid-gas interface is enhanced when both inner and outer air are present, thus increasing the instability. Swirling liquid sheets subject to combination of inner and outer axial air streams (Fig. 8) produce higher growth rates than liquid sheets swirling in quiescent gas medium (Fig. 3) due to increase in the relative velocities and the combined effect of centrifugal and aerodynamic forces. Higher air velocities would correspond to air blast atomization while lower air velocities would resemble a simplex atomizer configuration. The effect of combination of inner and outer air swirl in the presence of their corresponding axial velocities for swirling liquid sheets is shown in Fig. 9 respectively. In order to determine the effect of gas swirl, Fig. 9 is compared with Fig. 8, which consists of purely axial gas velocities. It can be concluded that swirl imparted to inner and outer gas streams have contrasting effects on the instability of swirling liquid sheets. This phenomenon can be explained as follows. The centrifugal force due to liquid swirl at the outer interface tends to push a perturbed interface further outward and exhibits a destabilizing effect. The pressure exerted on the outer interface by the swirling gas is higher than that at the unperturbed interface and hence tend to push the perturbed sheet back to its undisturbed state. Hence outer gas swirl has a stabilizing effect on a swirling liquid sheet. At the inner interface, the combined effect of the centrifugal forces due to liquid swirl which is of free vortex type and inner gas swirl which has a solid body rotation profile, increase the amplitude of perturbation. Thus, inner gas swirl has a destabilizing effect on a swirling liquid sheet. However, the range of axial wave numbers remains unaffected due to the effect inner and outer gas swirl when compared with liquid sheets subject to purely axial gas velocities. Primary break up length, ligament diameter and droplet diameter for Fig. 9 are decreases compared to Fig. 3 and improves combustion and reduces emissions and fuel consumption. So Fig. 9 has a shorter Primary break up length compared to Fig. 3. Also ligament diameter and droplet diameter of Fig. 9 is shorter than Fig. 9. The result is visible by comparing Fig. 4 to 6 with Fig. 10 to 12.

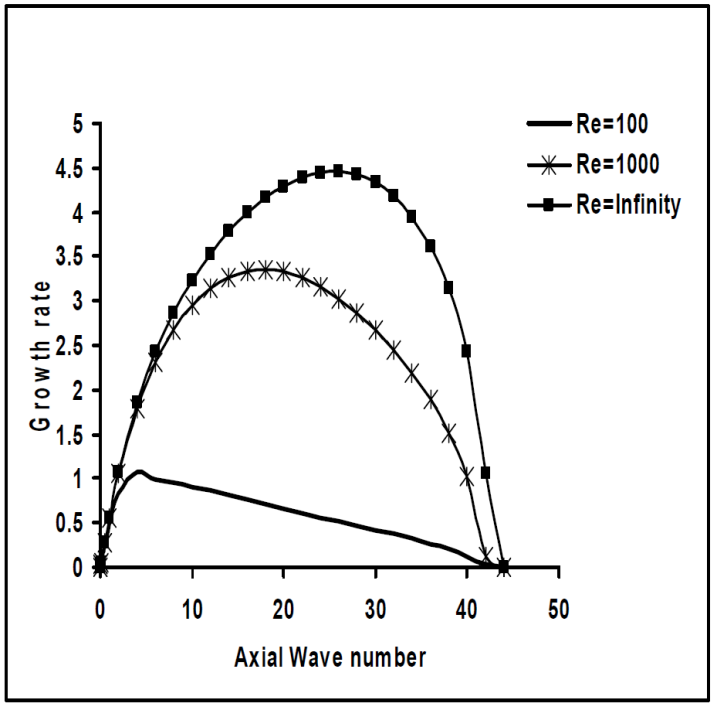

Fig. 8: Dispersion diagram at $We_l = We_s = 1000, We_i = We_o = 30$, $g_i = g_o = 0.00123$, $h = 0.95$

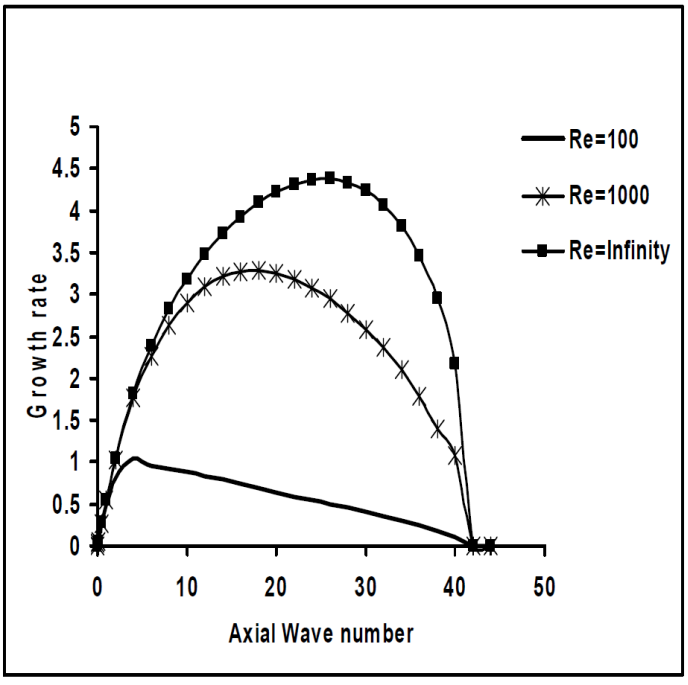

Fig. 9: Dispersion diagram at $We_l = We_s = 1000, We_i = We_o = We_{si} = We_{so} = 30$, $g_i = g_o = 0.00123$, $h = 0.95$

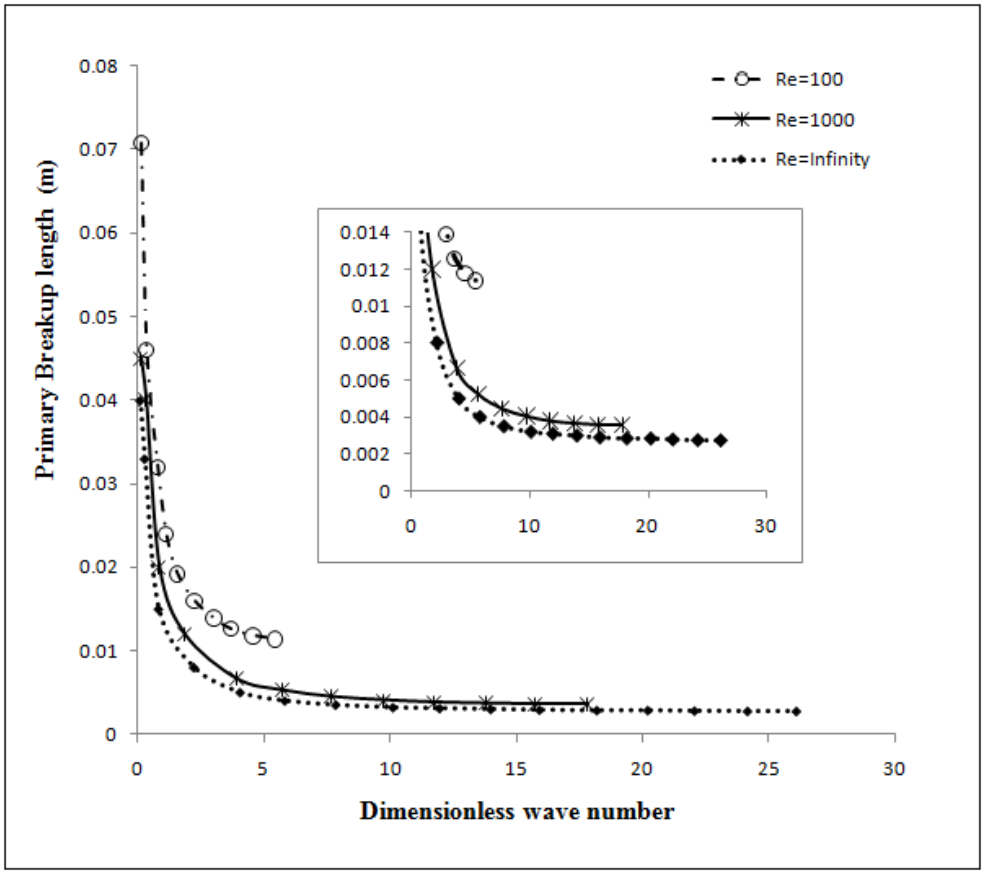

Fig. 10: The Effect of Liquid Viscosity on the primary break up of spray at $We_l=We_s=1000$, $We_i=We_o=We_{si}=We_{so}=30$, $g_i=g_o=0.00123$, h=0.95

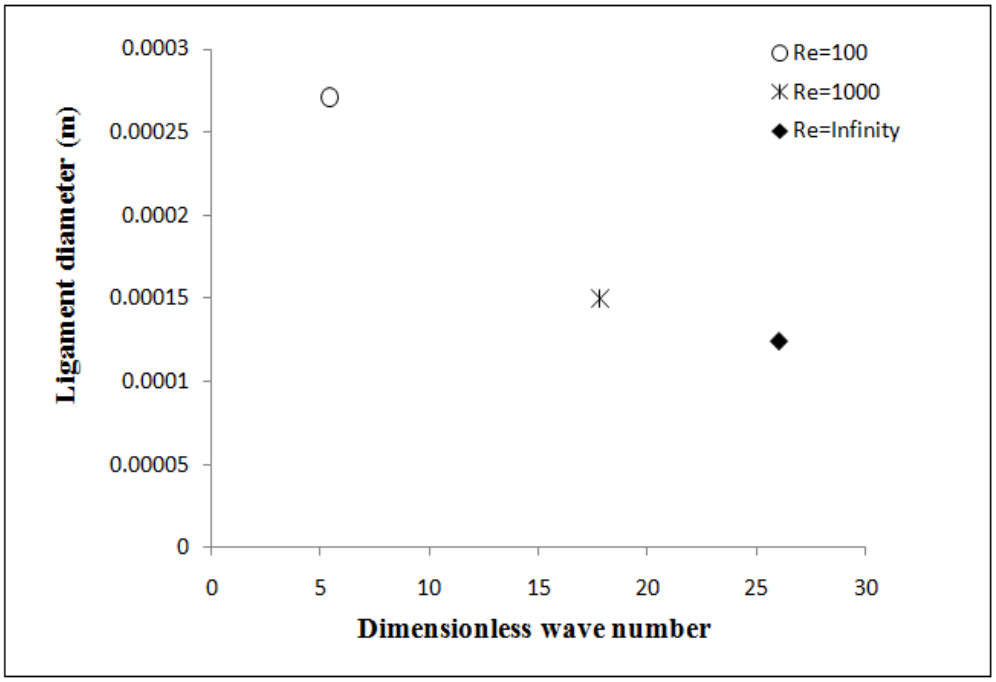

Fig. 11: The Effect of Liquid Viscosity on Ligament diameter at $We_l=We_s=1000$, $We_i=We_o=We_{si}=We_{so}=30$, $g_i=g_o=0.00123$, h=0.95

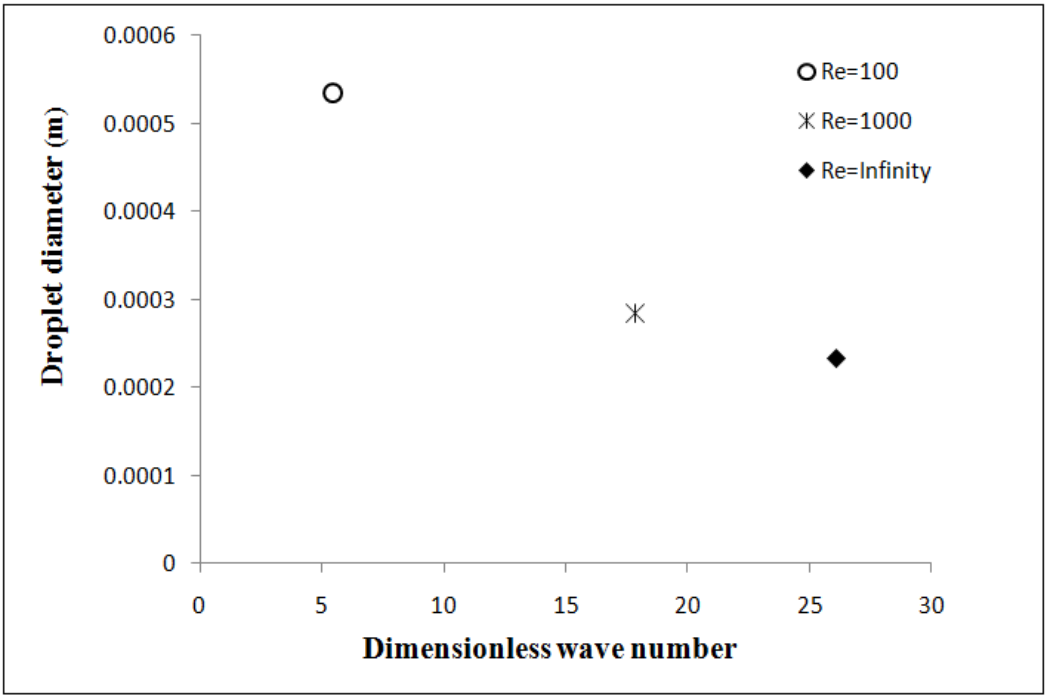

Fig. 12: The Effect of Liquid Viscosity on Droplet diameter at $We_l=We_s=1000$, $We_i=We_o=We_{si}=We_{so}=30$, $g_i=g_o=0.00123$, h=0.95

4. Conclusions

By varying the value of the axial wave number, we solved the root with the maximum imaginary part that represented the maximum growth rate of disturbance corresponding to the most unstable wave number.

From this study, we have drawn the following conclusions:

1- The maximum growth rate increases with Reynolds number.

2- Higher liquid velocity would lead to shorter breakup lengths and smaller droplets.

3- With increasing the wave growth rate, Primary break up lengths and ligament diameter are reduced and thus the droplet diameter decreases.

4- Liquid viscosity has a negative effect on the Primary break up lengths and it causes the increasing Primary break up length, ligament diameter and droplet diameter.

5- Liquid viscosity increasing tends to decrease both the growth rate and the most unstable wave number.

6- The damping effect of viscosity is significantly higher for a swirling sheet compared to a purely axially moving sheet.

7- Liquid swirl promotes instability at high Weber numbers.

8- Swirl imparted to inner and outer gas streams have contrasting effects on the instability of swirling liquid sheets.

9- Outer gas swirl has a stabilizing effect on a swirling liquid sheet.

10- Inner gas swirl has a destabilizing effect on a swirling liquid sheet.

11- Gas swirl causes the decreasing Primary break up length, ligament diameter and droplet diameter compared to a liquid sheet with both axial and swirl velocity.

12- The combination of inner and outer air is more effective in destabilizing swirling liquid sheets than liquid sheet with both axial and swirl velocity.

Reference

[1]. E.P. HERRERO, E.M. DEL VALLE, M.A. GALAN, *Instability study of a swirling annular liquid sheet of polymer produced by air-blast atomization*, Chemical Engineering Journal, 2007; 133.1: 69-77.

[2]. S.P. LIN, *Breakup of liquid sheets and jets*, Vol. 120. Cambridge, England: Cambridge University Press, 2003.

[3]. W.A. SIRIGNANO, C. MEHRING, *Review of theory of distortion and disintegration of liquid streams*, Prog. Energy Combustion, Sci. 2000; 26: 609–655.

[4]. M.V. PANCHAGNULA, P.E. SOJKA, P.J. SANTANGELO, *On the three-dimensional instability of a swirling, annular, inviscid liquid sheet subject to unequal gas velocities*, Phys. Fluids, 1996; 8: 3300–3312.

[5]. Y. LIAO, S.M. JENG, M.A. JOG, M.A. BENJAMIN, *Advanced sub-model for airblast atomizers*, J. Propulsion Power, 2001; 17: 411–417.

[6]. C. MEHRING, W.A. SIRIGNANO, *Non-linear capillary waves on swirling, axisymmetric free liquid films*, Int. J. Multiphase Flow, 2001; 27, 1707–1734.

[7]. F. CHEN, J.Y. TSAUR, F. DURST and K. SAMIR, *On the axisymmetry of annular jet instabilities*, J. Fluid Mech, 2003; 488: 355-367.

[8]. A.A. IBRAHIM, M.A. JOG, S.M. JENG, *Effect of liquid swirl velocity profile on the instability of a swirling annular liquid sheet*, Atomization and Spray, 2006; 16: 237–263.

[9]. P.K. SENECAL, D.P. SCHMIDT, I. NOUAR, C.J. RUTLAND, R.D. REITZ, M.L. CORRADINI, *Modeling High-Speed Viscous Liquid Sheet Atomization*, Int. J. of Multiphase Flow, 1999; 25: 1073-1097.

[10]. N. DOMBROWSKI, PC. HOPPER, *The effect of ambient density on drop formation in sprays*, Chem Eng Sci, 1962; 17: 291-305.